Journal of Energy Storage 142 (2026) 119509

Contents lists available at ScienceDirect

Journal of Energy Storage

journal homepage: www.elsevier.com/locate/est

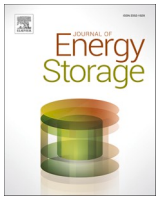

Research papers

Importance of reactor design on efficient utilisation of thermochemical heat storage materials for background space heating

S. Hosouli [a,*], R.J. Sutton [b], J. Searle [b], E. Jewell [b], J. Elvins [b]

[a] Faculty of Engineering, Computing and the Environment, Kingston University London, UK
[b] Faculty of Science and Engineering, Swansea University, Fabian Way, Swansea, Wales, UK

ARTICLE INFO

Keywords:
Salt in matrix
Thermochemical
Calcium chloride
Reactor design
CO_2 analysis

ABSTRACT

Thermochemical storage materials allow harvesting and storage of thermal energy (e.g. from industrial waste heat) potentially reducing emissions to atmosphere and time-shifting the hitherto wasted energy for later use in heating buildings. Reported thermochemical storage densities vary widely, with many studies overestimating laboratory-scale data when linearly scaling to practical reactor sizes. Presently, an experimental and design model analysis has been carried out on a stacked bed reactor using varying material depths to evaluate thermal performance, energy storage capacity and environmental impact in a modelled industrial scenario. Using a bench top reactor, the depth of the thermochemical storage material (CaCl2/ vermiculite) was varied between 30 and 60 mm with variations in input flow rate of moist air between 5 and 40 LPM. Maximum temperature uplift (11–13 °C) and energy densities (80–110 kWh/m^3) were obtained with 30–40 mm of material with high flow rates. The experimental results were utilised in a design simulation to identify the optimum thermodynamic and low carbon impact material depth and inter gap spacing in order maximise the effective reactor storage density. Multiple 30 mm layers with a small interlayer gap provided the best energy density (59.2 kWh/m^3), opposed to fewer 60 mm layers with a large interlayer gap (15.1 kWh/m^3). Thermal performance of a single space cabin heated via harvested industrial waste heat is modelled, with subsequent LCA analysis to determine carbon impact compared with heating via electricity and gas alternatives. The carbon impact varies with reactor design and operational use, but cabins utilised over multiple years show a significantly improved carbon footprint.

1. Introduction

The future landscape of space heating needs to be drastically different if the defined decarbonisation targets are to be achieved [1] and energy is to be utilised in an economic and efficient manner. An almost total reliance on combustion of natural gas and oil will have to be diversified to a combination of sources such as heat pumps, solar thermal technologies (Evacuated tube, Transpired solar collector etc.), district heat networks, waste heat recovery and alternative gases. Each of these will provide unique challenges to be adopted effectively and can be made more efficient when coupled with heat storage technologies either through the reduction in peak generation requirements, enhancing the distribution capability or addressing the generation/utilisation mis-match [2]. Industrial waste heat provides an ideal resource for exploitation, and this has been recognised and acted upon for many decades with many high temperature waste streams that would eventually be vented to atmosphere, being reclaimed for use within local processes. Traditionally, this is achieved via heat exchangers and hot water generation or by the conversion into electricity using steam generators [3]. However, the low temperature resource (up to ≈250 °C) is less exploited due to inefficiencies of capture, prohibitive economics or geographically local use cases. The Department of Energy & Climate Change (DECC) reported that across the UK around 48 TWh/yr of industrial waste heat (IWH) is generated and the majority is still lost to atmosphere [4]. Of this the reported waste heat the amount in low temperature ranges is from 16.7 TWh/year to 17.4 TWh/year [5]. Hence, the ability to capture low grade waste heat and use it purposefully, could offset the primary generation requirements and therefore impact upon the carbon footprint and economic potency of an industrial site.

Historically, the main technology for heat storage in domestic and industrial scenarios is sensible heat storage via tank thermal energy storage (typically water) and solid state thermal storage (typically rock, concrete or cement) [6]. However, sensible heat stores have a low

* Corresponding author.
E-mail address: S.Hosouli@kingston.ac.uk (S. Hosouli).

https://doi.org/10.1016/j.est.2025.119509
Received 7 April 2025; Received in revised form 3 October 2025; Accepted 16 November 2025
Available online 22 November 2025

storage capacity (~60 kWh/m^3 at a temperature difference of 50 °C) and suffer from relatively high heat losses to the ambient during the storage period [7]. Compact and long-term storage processes will play an important role in future energy systems and reduced heat losses and high specific storage capacities are key technical characteristics for future energy storage developments. Of the available forms of heat storage (sensible, latent and thermochemical), thermochemical storage (TCS) is seen as the most credible long-term option as the higher storage densities will lead to a reduced volume and therefore a more efficient space utilisation within the application [8,9]. However, TCS has more complexity in comparison with sensible or latent heat storage and therefore requires further research on material development and reactor (system) design to reach commercialization stage [10].

TCS can store energy through the chemical bonds of suitable materials with minimum energy loss for long term applications (under the correct conditions) and typically have a high energy storage density. Research in low-temperature TCS has been mainly focused on material development and optimization over the last decade [9,11,12]. In reversible chemical reactions, a large amount of energy is generated because of an exothermic synthesis reaction [13]. Dehydration of salt hydrates, metal hydrates, metal hydroxides, deammoniation of ammonium chlorides and decarboxylation of metal carbonates are among the reversible chemical solid/gas reactions for TCS [9,14]. One of the most researched variants of TCS material for residential applications is hydrated salt systems which operate through the dehydration and hydration of chemical salts to store and release thermal energy (~high energy density 400–870 kWh/m^3) via *endo-* and exothermic reactions at low turning temperature (<150 °C) [9].

In general, reversible reaction of a salt hydrate in TCS system can be represented by Eq. (1).

$$Salt \bullet nH_2O_{(s)} + Heat \leftrightarrow Salt_{(s)} + nH_2O_{(g)} \quad (1)$$

The reversible reaction can take place in different steps at different desorption temperatures with a possibility of intermediate hydrate formation within the system [15].

Several studies have been conducted to investigate various kinds of TCS material ($MgSO_4$, Na_2S, $MgCl_2$, $CuSO_4$, $SrBr_2$, Al_2SO_4 and $CaCl_2$) and their composites (salt within an inert or active material) [16].

The de/hydration reactions for Magnesium sulphate ($MgSO_4$), $MgSO_4{\cdot}7H_2O$ and $MgSO_4{\cdot}2H_2O$ were investigated examining material crystal and grain-scale properties [17], heat release temperature [18], effect of moist air flow [19], water vapour pressure [18,19], kinetics of hydration [20] and cyclability [21]. The application of sodium sulphide (Na_2S) as a heat storage medium for domestic purposes was investigated initially by [22]. Intermediate hydrates formation, operating under vacuum and the perceived main drawbacks of Na_2S were investigated by other researchers [23,24]. As a promising material, magnesium chloride ($MgCl_2$) has been investigated by numerous research groups focusing upon its decomposition mechanism [25], instability at high and low temperature [26], kinetics [27] and cyclability [28]. Due to safety measures (toxicity) and low cyclability of copper sulphate ($CuSO_4$) it does not seem to be a suitable choice for TCS [29]. However, many studies have been conducted on $CuSO_4$. [30] studied application of copper sulphate in an open system configuration in a lab reactor and reported maximum temperature lift of 11 °C for a hydration temperature of 40 °C. Further to this [29] copper sulphate stability over multiple cycles was investigated and a significant decrease in the kinetics after 13 cycles was reported. The reaction from the hexahydrate to the monohydrate in strontium bromide ($SrBr_2$) was studied by many researchers due to the excellent stability of the salt over multiple de/hydration cycles and relatively high energy density of material [31–33]. However, its high cost is the main drawback of strontium bromides use in large systems with few cycles per year. Aluminium sulphate (Al_2SO_4) has been studied in detail at 13 mbar of water vapour pressure for dehydration and hydration temperature of 150 and 25–50 °C, respectively. Significantly, a too low temperature lift is also reported for aluminium sulphate [19] leading to limited further studies.

One attractive material is $CaCl_2$ which benefits from being low cost, applicable to low temperature thermal charging and readily reacts with moisture in the air to release energy, [34–37]. Standard enthalpy of formation ($\Delta_f H^{\ominus}_{298}$) for calcium chloride hexahydrate and calcium chloride dihydrate is −2608.01 kJ/mol and − 1403.98 kJ/mol, respectively [38]. Therefore, in hydrating from the $\bullet 2H_2O$ state to the $\bullet 6H_2O$ state, 1204.03 kJ/mol are released. The dehydration of $CaCl_2 \bullet 6H_2O$ to $CaCl_2$ proceeds in 3 reaction phases. The respective decomposition phases are represented by Eq. (2) [39].

$$CaCl_2{\cdot}6H_2O_{(s)} \rightleftarrows CaCl_2{\cdot}4H_2O_{(s)} + 2H_2O_{(g)} \rightleftarrows CaCl_2{\cdot}2H_2O_{(s)} + 4H_2O_{(g)} \rightleftarrows CaCl_{2(S)} + 6H_2O_{(g)} \quad (2)$$

Reported assessments of the storage density of $CaCl_2$ vary considerably (0.43 to 2.8 GJ/m^3) between studies [10,14,40,41]. Analytical laboratory analysis on small quantities, measure values towards the upper limit while the impact of scale reduces this appreciably such that even laboratory reactors are 15 % to 26 % of these high theoretical values (2.8 GJ/m^3). This reduction in energy density has a direct impact on the viability of the technology as real-world thermal storage solution [42]. There is a growing body of literature focused upon the upscaling of TCS materials and systems from lab-based reactors through to demonstration sized systems [43,44]. The configuration of these systems varies with stacked bed, fluidized bed, entrained bed [45] and revolving drum [46].

Porous materials as host matrices (desiccants) such as inherent adsorbents (silica gel and zeolites) [47,48], high porosity materials (activated carbon, natural rocks) [49–52] and high thermal conductivity materials (expanded natural graphite) [53,54] have been used widely by researchers to improve stability and heat/mass transfer performance of hydrated salts. Salt within the pore structure of a host matrix called Salt In Matrix (SIM). Natural minerals, such as vermiculite (VM) have relatively low cost and offer the advantages of porous structure. Although VM as a matrix has a weak adsorption capacity for water vapour, it has several advantages over other host matrices. VM with microporous structure can control and stabilize the output temperature under certain working conditions. It is conducive to adsorbate transportation and provides support for composite stability. Therefore, VM retains the salt solution and prevents its leakage because of excessive water adsorption [55]. Our previous study on the selection of salt impregnated desiccant matrices for open TCS revealed that, at low-humidity environment VM-$CaCl_2$ SIM (VM as the matrix and $CaCl_2$ as the salt) shows high adsorption capacity and has a more stable structure from the perspective of porosity change [49].

Previous work has highlighted the high affinity of $CaCl_2$ for water, which enables rapid release of thermal energy [56,57] but this affinity comes at the expense of deliquescence of the $CaCl_2$ near the initial moisture / salt point of contact [57–59]. This leads to poor utilisation of the salt with SIM further long the air transit path remaining dry, and therefore restricting energy release as the deliquescence provides an endothermic sink at the inlet to the reactor. There is therefore a balance which must be addressed where the path length and residence time are minimized for efficient material utilisation, but the geometric complexity and overall reactor energy density are not prohibitively impacted. Hence the system design needs to consider the free space within a reactor, which aids overall utilisation but does not contribute to the net energy density.

System design and reactor configurations are critical factors in development of TCS for space heating applications. As mentioned before, despite numerous studies on SIM pairs and reversible chemical reactions for TCS, real-world thermal storage solutions and understanding the effect of system design and reactor configurations in large scale remains relatively sparse [60]. In a conventional large diameter packed bed (fixed bed) reactor design, the system requires a large

pumping power due to the high drag between the fluid and the particles and enabling improved performance if heat transfer rate is poor [61,62]. In order to optimize the proportion of free space and SIM mass in the reactor and consequently the introduction of TCS into the commercial arena, a stacked bed reactor model was created to match the demands of the customers. Fundamental to the validation of the model were experimental results taken from a laboratory scale reactor, where the volume and height of the SIM was varied over a range of operational flow rates.

TCS type systems are thought to provide the ability to decouple the generation and use points of thermal energy, therefore delivering the efficient transport of energy without the associated heat losses incumbent in district heat networks or sensible/latent thermal energy storage systems. Application of TCS for reusing and recovering of IWH can improve the competitiveness of this energy resource by yielding a better capacity factor and solving the mis-match between IWH and heat demand [63]. Furthermore, mobile off-site TCS can be used to address geographic decoupling of heat supply and demand by being transportable from the source location [64]. In this paper, the use of TCS, based on VM-$CaCl_2$, for IWH utilisation has been investigated through the reuse of waste heat via a space heating system deployed within a temporary modular building site office. The work assumes a constant waste heat input, based upon a minimum requirement for the annual heat load, to meet the demand of the building, which is captured from local processes and discharged over a 10 h period representing a single days operation. Furthermore, an assessment of global warming potential of the proposed system for background space heating has been compared to a conventional gas and electric heating systems using scenarios where firstly the TCS is used once and then replaced and secondly where the TCS is discharged over multiple days until the stored energy is depleted.

2. Materials & methodology

The current investigations were completed using a vermiculite / calcium chloride composite (Salt/Matrix ratio of 2:1) synthesised via the Incipient Wetness Technique (IWT) [65,66]. The technique utilises a materials natural liquid absorption capacity (i.e. capillarity) to fill the pore structure (Vermiculite) with the desired salt solution ($CaCl_2$ solution).

Vermiculite $(Mg,Ca,K,Fe^{2+})_3(Si,Al,Fe^{3+})_4O_{10}(OH)_2{\cdot}4H_2O$ was acquired commercially from a supplier to the horticultural industry with a nominal particle size of 2–8 mm. Anhydrous Calcium Chloride (purity 99.99 %) was sourced from Sigma Aldrich from which a saturated $CaCl_2$ solution to ≈100 % of the matrix pore volume (V_p [cm^3/g]) was produced based on total sample mass (m_m [g]) and maintained at 20 °C. The volume of the saturated salt solution is given by $V_p \times m_m$. Prior to synthesis, the vermiculite was pre-filtered to remove loose fines and the pore volume determined using Mercury Intrusion Porosimetry (MIP). During synthesis a predetermined volume of $CaCl_2$ solution was systematically applied to a known quantity of vermiculite using a fine spray technique. Even distribution was ensured by gently turning the vermiculite after each pass of the spray equipment. Upon completion, the TCS material was dried at 120 °C for 24 h producing the final materials with the salt at the dihydrate state (Fig. 1(a)). Fig. 1(b) shows SEM of obtained salt in matrix (SIM) material at 2:1 salt to vermiculite ratio synthesis via IWT.

Material thermodynamic performance was examined using the experimental apparatus shown in Fig. 2. Dry compressed air (7 % Relative Humidity (RH) at 20 °C) was passed through a flowmeter and into a Dreschel bottle allowing control of both the flow rate and the final moisture level in the air at 17 g/m^3. The moisture input level was assessed during commissioning and found to be consistent for each flow rate (±0.5 g/m^3) with a water volume maintained at 2 l.

Table 1 shows operational parameters for each volume of TCS material (SIM height 30–60 mm) subjected to moist air flow rates of between 10 and 40 lpm. Layers below 30 mm were not considered as particle size makes them difficult to specify consistently and there is an additional thermal mass and physical engineering complexity associated with many multiple thin layers, such that the thickest efficient layer is more optimal from an energy density and system complexity consideration.

The TCS material was housed in a bespoke constructed transparent

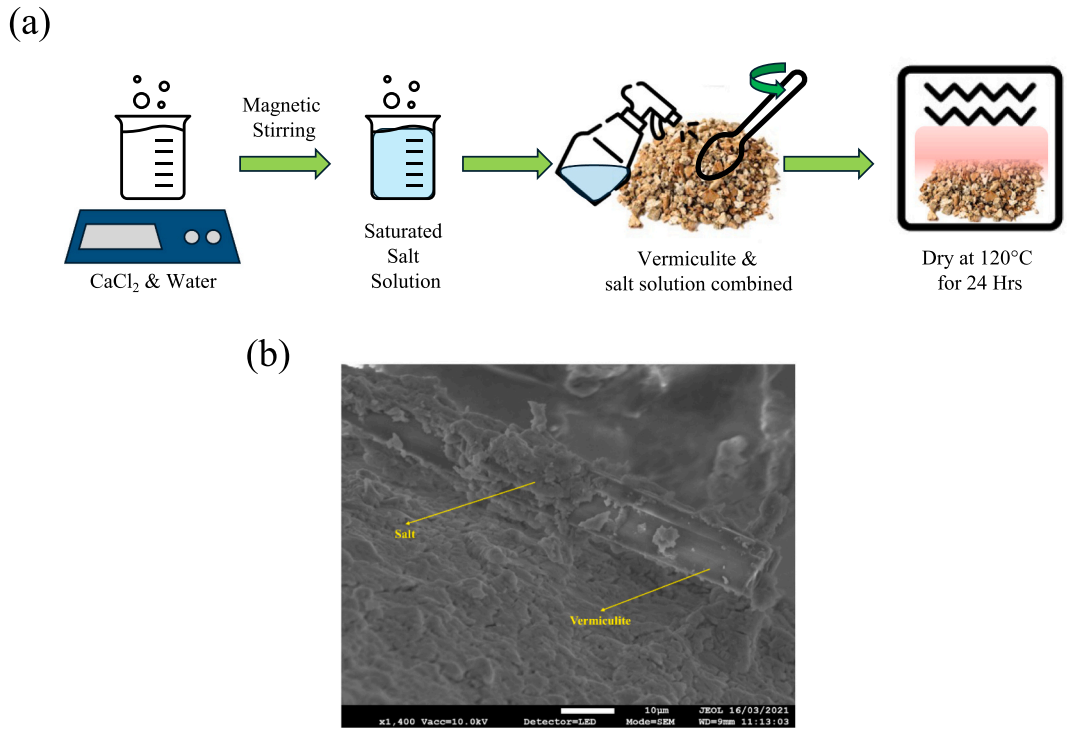

Fig. 1. (a) Schematic illustration of vermiculite / calcium chloride composite (SIM) synthesis via IWT (b) SEM of salt in matrix (SIM) material at 2:1 salt to vermiculite ratio.

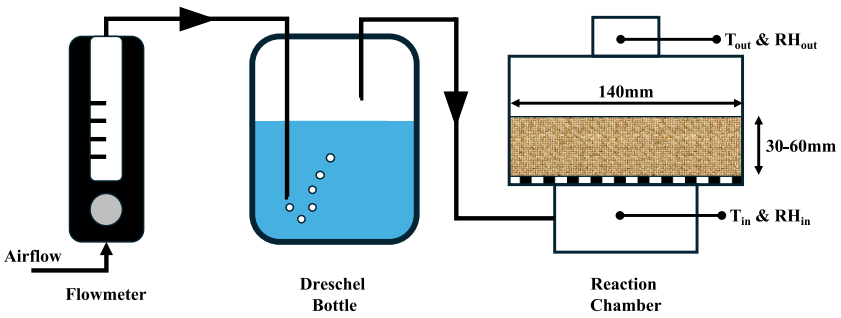

Fig. 2. Experimental laboratory setup.

Table 1
Operational parameters investigated to reach full reaction from dihydrate to hexahydrate.

Volume flow rate (lpm)	H_2O supply rate (g/h)	Time to supply to full hydration (hours)			
		30 mm	40 mm	50 mm	60 mm
10	10.92	7.7	10.3	12.8	15.4
20	21.84	3.9	5.1	6.4	7.7
30	32.76	2.6	3.4	4.3	5.1
40	43.68	1.9	2.6	3.2	3.9

polypropylene chamber of dimensions 140 × 140 × 100 mm. The chamber contains a perforated base allowing uniform distribution of the inlet air. Inlet and exit temperatures were monitored over a 10 h period by type K thermocouples (accuracy of ±1.5 °C) with the primary figure of merit being the temperature uplift experienced by the air. Experiments were repeated and averages taken to ensure accuracy. The air moisture content was measured using a TE-HPP805C031 RH sensor with relative accuracy of ±2 % RH. Uncertainty is evaluated for all the measured values by considering both Type A and Type B errors for experimental data measurement and instrument characteristics uncertainty, respectively [67]. For propagation of errors in the derived parameters, the combined standard uncertainty is used, based on the sum-of-the-squares method. A coverage factor of k = 2 is used in reporting the expanded uncertainty to provide 95 % level of confidence [68].

The thermal uplift results obtained in the laboratory reactor were used to predict the effectiveness of a theoretical stacked bed reactor (Fig. 3) which has been postulated as a possible generic reactor design. In this design, each bed of material has an individual moist air supply which can be controlled independently. The principle of operation being that each layer, or multiple layers, can be discharged, then isolated and replaced by fresh un-hydrated TCS material as they are spent. The multi-layer approach allows for parallel operation when heat demand is high, but with in-built redundancy such that the risk of zero heat output is minimized.

The total reactor height (h_r) is given by:

$$h_r = \sum_{1}^{n} \left(h_b + h_{in} + h_{out} + h_p + h_{tcs} \right) \quad (3)$$

where h represents the height and the subscripts b, in, out, p and tcs refer to the solid base, gap at input, gap at output, porous grill and thermochemical storage material respectively. In all designs of theoretical stacked bed reactor, $h_{in} = h_{out}$. Table 2 shows design parameters for single layer of theoretical stacked bed reactor.

Table 2
Design parameters for single layer of theoretical stacked bed reactor.

Layer name	Symbol	Height [mm]
Solid base	h_b	2.5
Gap at input	h_{in}	10, 20, 30,40, 50, 60, 70
Porous grill	h_p	2.5
Gap at output	h_{out}	10, 20, 30,40, 50, 60, 70
Thermochemical storage material	h_{tcs}	30, 40, 50, 60

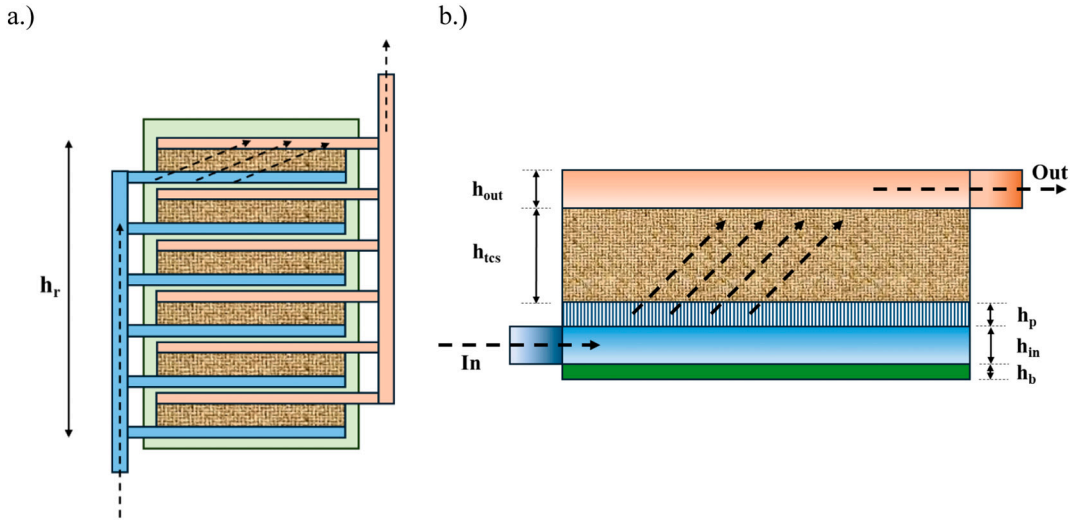

Fig. 3. Stacked bed reactor model used to assess storage density a) The stacked bed reactor model, showing the overall multi-layer assembly b) A detailed schematic of a single layer's components and height parameters.

3. Results and discussion

3.1. Efficient utilisation of SIM

The thermal energy liberation from the SIM and the subsequent temperature rise over the discharge period at the exit of reactor follows a pattern which is highly dependent upon the input air flow rate and SIM height. Fig. 4 shows the reactor exit thermal output profiles across the flow rate range for each TCS material height in the reactor.

Two profiles of energy release are observed depending upon the flow rate with either a rapid increase to maximum, followed a steady reduction in temperature at elevated flow rates or a slower increase to peak output (albeit much lower than the rapid scenario) where the temperature is then maintained over the experimental duration at the slower flow rates.

At a constant SIM height (30, 40, 50 and 60 mm) and highest flow rate (40 lpm), the rate of temperature uplift initially increases rapidly to a maximum value within 1 h and then reduces gradually over the next 9 h. At highest flow rate (40 lpm) and SIM height (60 mm), the temperature is maintained over the experimental duration and the rate of temperature loss following the peak is slower in comparison with SIM height of 30, 40 and 50 mm. A faster flow rate of moist air contains higher amount of humidity (energy liberating agents) and air (heat transport agents) per unit time [69]. Further to this, the utilisation of the available humidity is shown in Fig. 5. To quantify the efficiency of the reaction, the moisture utilisation was calculated. The difference between the inlet supply moisture concentration and the exit moisture concentration has been used to calculate utilisation of moisture by SIM. Moisture utilisation is defined as the percentage of the water vapour in the incoming air that is captured by SIM. It is calculated as the difference between the moisture concentrations (g/m^3) measured at the reactor inlet and outlet, divided by the inlet concentration. It is clear that, at 60 mm depth the peak utilisation (86 %) of available humidity is significantly higher than that of the 30 mm depth (43 %) and consequently the liberation of energy under these conditions will be maximised. Therefore, in all SIM heights (Fig. 4a–d) temperature uplift peak value and the rate of temperature loss following the peak is higher for higher flow rate (40 lpm) due to the increased amount of energy liberating agents, a higher amount of heat transport agents and enhanced utilisation of the available moisture within the air flow.

In order to assess the thermal uplift profiles and further understand their implications, key thermal output characteristics can be examined. Fig. 6 shows these indicators for the laboratory reactor. Increasing the air flow rate has a positive effect on the maximum temperature (Fig. 6 (a)) and mean temperature (Fig. 6(b)). The highest peak temperature is obtained with the thinnest layer of material, 30 mm (Fig. 6(a)) and the additional height of material also does little to increase the mean temperature rise over the 10 h period, Fig. 6(b).

The overall energy evolved (E_{EV}), calculated by integrating the product of the mass flow, temperature uplift and specific heat over time (Eq. (4)).

$$E_{EV} = mC_p\Delta T_{Ave} \tag{4}$$

The error $u_{E_{EV}}$ associated to overall energy evolved is calculated by Eq. (5):

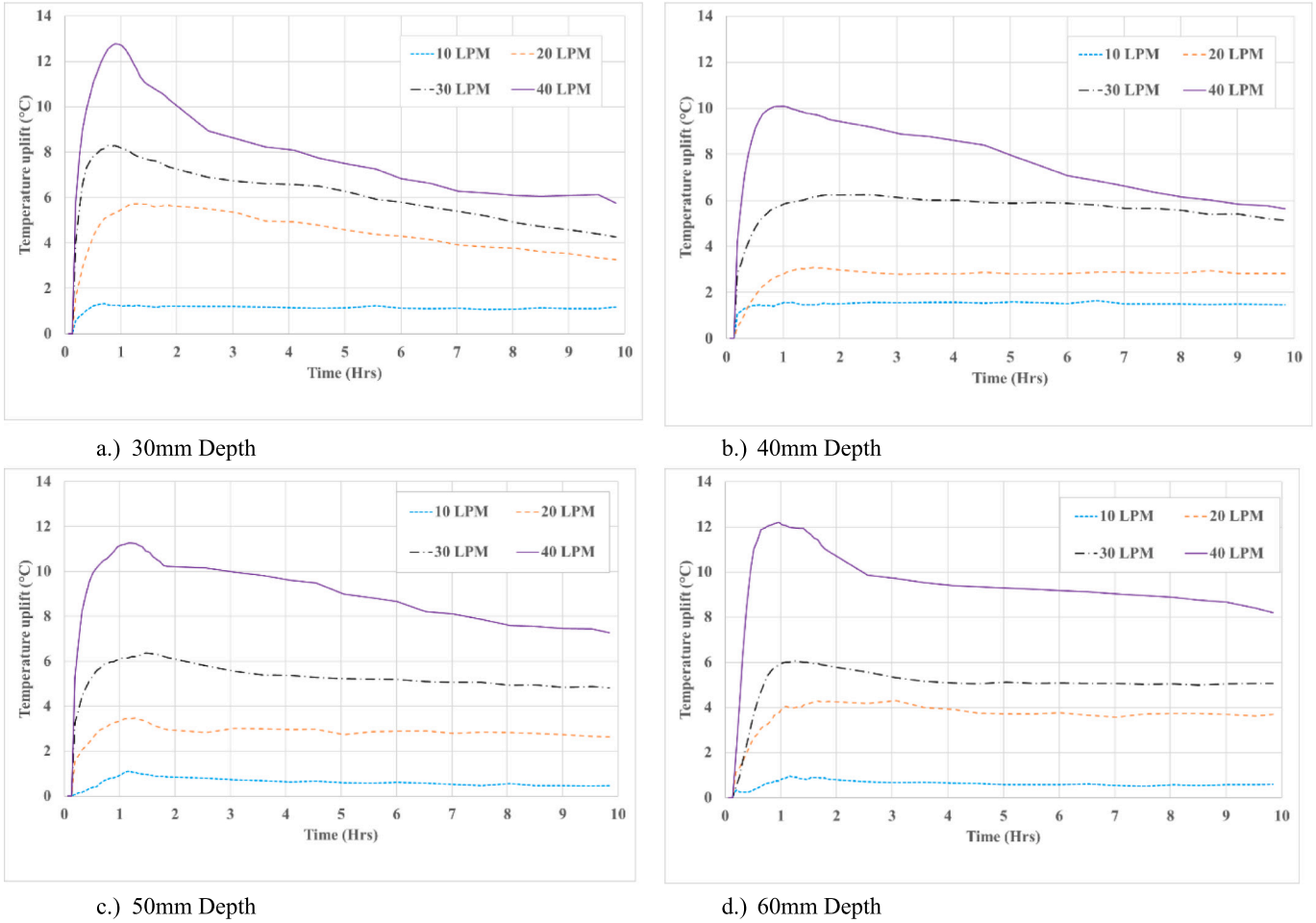

Fig. 4. Reactor exit thermal output profiles across the flow rate range for each TCS material height in the reactor.

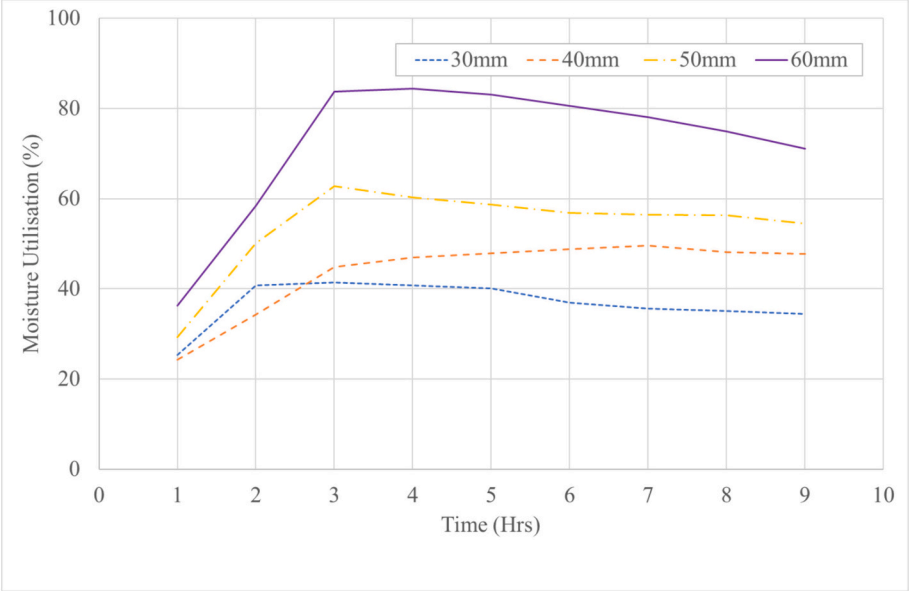

Fig. 5. Moisture utilisation for each SIM height (30, 40, 50 and 60 mm) at 40 lpm.

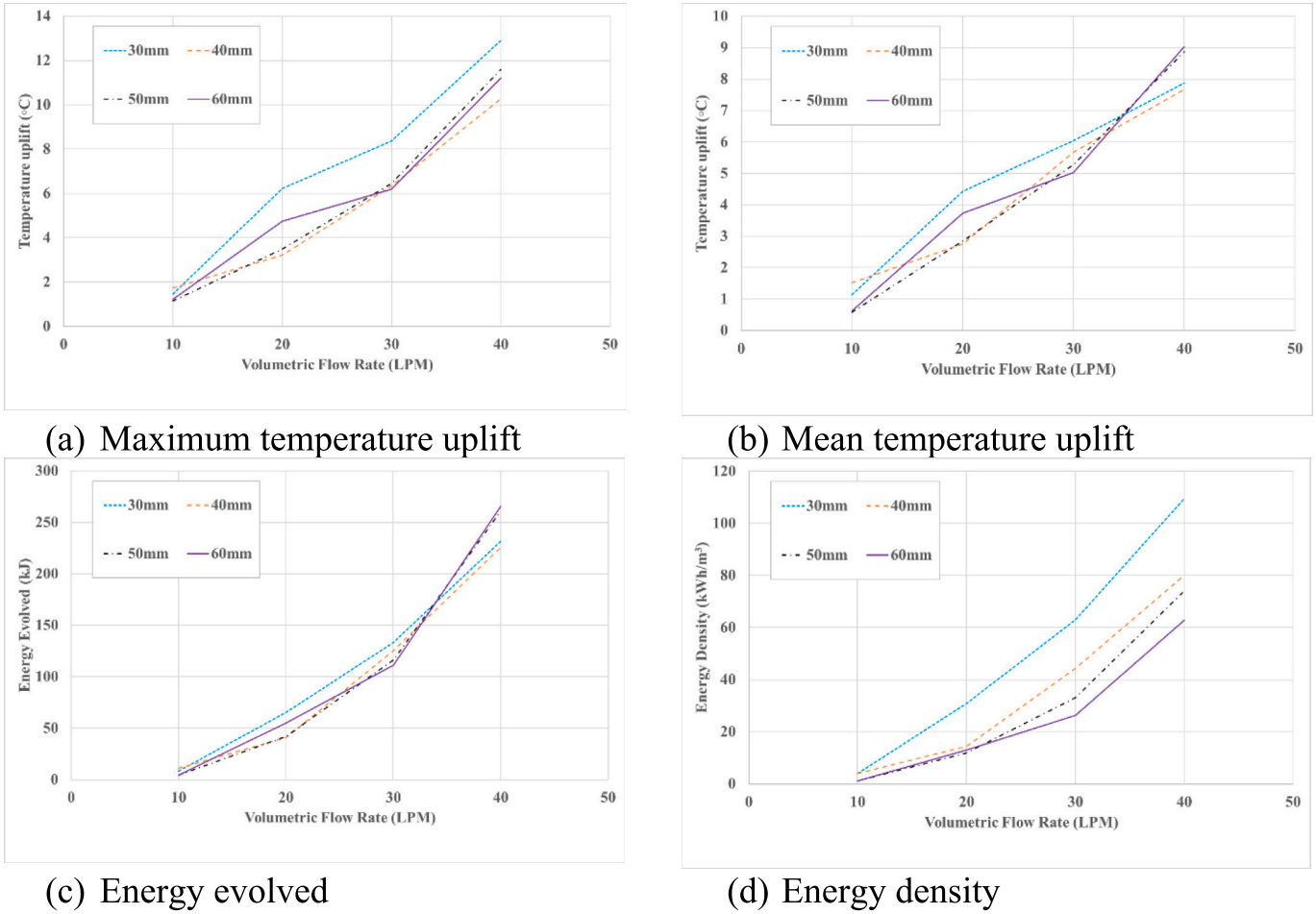

Fig. 6. Key thermal performance indicators for the laboratory reactor (a) Maximum temperature uplift, (b) Mean temperature over 10 h, (c) Total energy evolved and (d) Effective energy density.

$$u_{E_{EV}} = \sqrt{\left(\frac{\partial E_{EV}}{\partial m}u_m\right)^2 + \left(\frac{\partial E_{EV}}{\partial C_p}u_{C_p}\right)^2 + \left(\frac{\partial E_{EV}}{\partial \Delta T_{Ave}}u_{\Delta T_{Ave}}\right)^2} \quad (5)$$

where u_m, u_{Cp}, $u_{\Delta TAve}$ are the errors related to the different factors involved in overall energy evolved. The total uncertainty values for the thermal loss in tests are in the order of Joules. For temperature difference the maximum absolute error is 0.9 °C and absolute expanded uncertainty with coverage factor of 2 is 1.8 °C. For overall energy evolved and energy density, the maximum relative error is 5.13 % for both and maximum absolute expanded uncertainty with coverage factor of 2 is 1.8 kJ and 0.8 kWh/m^3, respectively.

Over the 10 h experimental period, E_{EV} shows no discernible advantage for a larger TCS material in the reactor, Fig. 6(c). The net result is that the energy density reduces as the thickness of material in the reactor increases, Fig. 6(d). This has significant implications for reactor design and the means by which real world reactors can be scaled. The material above 30 mm is inefficiently used and given the results in Fig. 6(c) that in certain areas it does not react at all after 10 h. This was evidenced by visual inspection of the SIM on the upper portion of the reactor which remained dry (Fig. 7). The initial vapour salt reaction occurs at the base of the reactor. The highest maximum (Fig. 6a) and mean (Fig. 6b) temperature uplift is associated with the 30 mm depth as the remainder of the unreacted salt acts as a thermal sink with a proportion of liberated energy being transferred into the unreacted bulk. The energy evolved in each case is similar, highlighting that there is portion of the bed above 30 mm which does not contribute a net positive impact on the energy which is released from the SIM, (Fig. 6c). A layer of the SIM towards the top of the (>30 mm) remains either unreacted or acts as a thermal sink and absorbs energy liberated further down the reactor. The net effect is that the SIM energy density reduces as the depth of SIM increases (Fig. 6d).

A primary finding from the experimental investigation is that the temperature uplift and the energy density of the material are governed by the height of the SIM, discharge time and moist air flowrate.

Moisture content at the top and bottom layer of each SIM height (Fig. 8) and visual observation indicates that the region near the inlet continues to gather moisture from the air without liberating energy. These observations result in defining the main determinants/factors affecting the performance of stacked bed reactor. The main factors associated with the decrease in performance are deliquescence of salt in SIM, intra particle pores being blocked, a quantity reduction of incident water vapour, a sink in the energy balance and increase in thermal mass

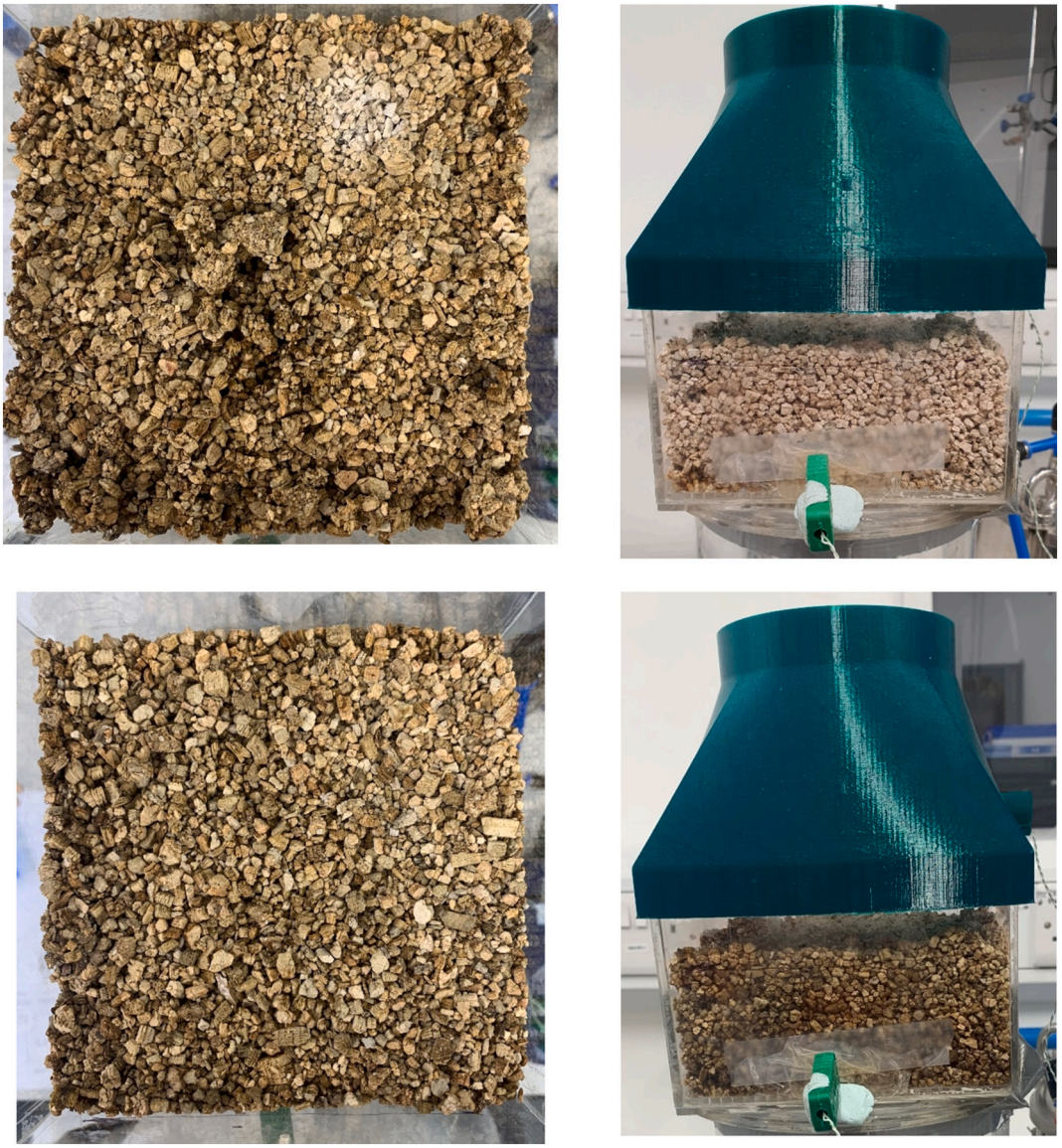

Fig. 7. Images of material which is over saturated at the bottom of a 60 mm height of reactor while remaining dry at the upper surface.

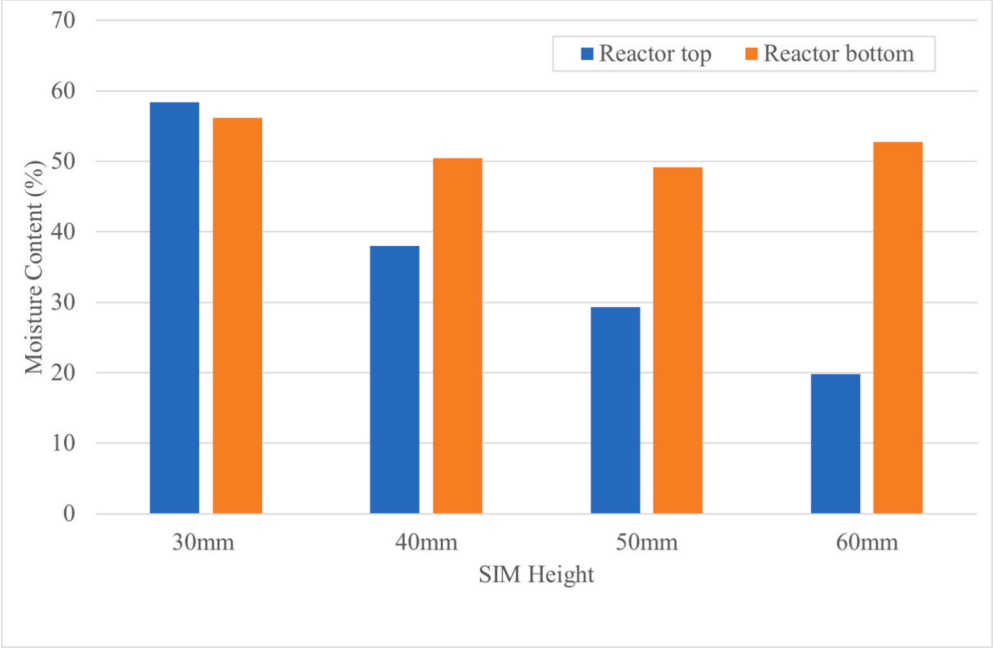

Fig. 8. Moisture content at top and bottom layer of each SIM height (30, 40, 50 and 60 mm) at 40 lpm.

of the system [70].

As the SIM height increases above 30 mm, the intra particle pores blocking effect increases due to the deliquescence of salt and formation of excess water on the SIM surface. This results in restrictions for the passage of the air through the SIM. Previous studies have shown that this excess water increases the thermal mass of the system and acts as a moisture harvesting agent from the inlet air reducing the quantity of water vapour which is available for reaction further downstream of the saturated SIM [70]. Furthermore, the temperature decreases due to enthalpy of vaporisation and its role as a sink in the overall energy balance. Results indicate that above a SIM thickness of 30 mm, energy density is lower than 30 mm (salt utilisation is poor) and the upper surface will remain dry due to the aforementioned factors.

Due to the discharge time of 10 h being insufficient to fully discharge the SIM of thickness above 30 mm, further experimentation was conducted to determine the maximum period of discharge for the 60 mm SIM depth. This would allow full utilisation of the SIM available, with a minimum temperature uplift of 5 °C selected as the operational cut off point. Since users turn their heating on and off at set times of the day two scenarios are detailed in Table 3, firstly a continuous discharge of the SIM and secondly an intermittent cycle where the air flow is on for a 2 h period and then off for 1 h, with this repeating to the experiment end. This experimentation determined that with continuous discharge, 43.07 h is required to achieve minimum target uplift temperature of 5 °C with a SIM thickness of 60 mm, with a resulting energy density of 247.7 kWh/m^3 (Table 3). After this period, moisture content difference between the top and bottom layer was significantly closer (60.2 % bottom and 50.8 % top) which was also confirmed by visual inspection. The required time for full discharge to while maintaining a target uplift temperature of 5 °C within the ON/OFF regime (2 h ON/1 h OFF) is 50.13 h of which 34.13 h is operational discharge time. Data for the average temperature uplift and energy density (shown in Table 3) is reported for the pure discharge time (34.13 h) for intermittent discharge cycle and shows greater moisture content at the top of the reactor, but reduced average temperature and energy density when compared to the continuous discharge scenario.

Table 3
Experimental data of fully discharge for the 60 mm SIM depth.

	Time maintaining uplift of >5 °C [hrs]	Average temperature uplift [°C]	Moisture content [%]	Energy density [kWh/m^3]
Continuous discharge cycle	43.07	9.3	Bottom: 60.2 Top: 50.8	241.7
Intermittent discharge cycle	50.13	8.2	Bottom: 60.2 Top: 54.4	195.9

3.2. Stacked bed reactor model for background space heating

To evaluate the potential of TCS type systems, a standalone heating system has been designed to be located within a portable cabin, acting as background heating during a working day scenario. In a stacked bed reactor, there are competing requirements. While higher material energy densities are found in thinner layers, the overall reactor energy density is reduced by the inactive volume of interlayer gaps, bases, and separators required for each layer. This trade-off informed the decision to set a lower experimental limit of 30 mm for the material depth. Layers thinner than 30 mm were not considered for two main reasons. Firstly, the added physical complexity and inert thermal mass from the increased number of support structures would have a negative impact on the reactor's thermal response. Secondly, due to the granular nature of the material (3–7 mm particles), very thin layers would be subject to significant surface variations (±2 mm), leading to large uncertainties in the actual material volume. Therefore, the research focused on identifying the thickest layer possible that ensured complete hydration, as this is most desirable for a practical application. Fig. 9 shows an open system design based on proposed stacked bed reactor model for space heating application which runs at atmospheric pressure, exchanges mass and energy with the surroundings. The reactor is modelled such that each layer operates individually, either sequentially such that each layer begins to discharge only when a previous layer has been fully discharged, or in parallel. Operationally two alternatives are considered to provide fully charged materials from the waste heat sources. Firstly, a cassette style system would enable easy replacement of spent systems via a manual exchange process. Secondly, assuming the point of end use is close to the waste heat source, controlled heat flow could be

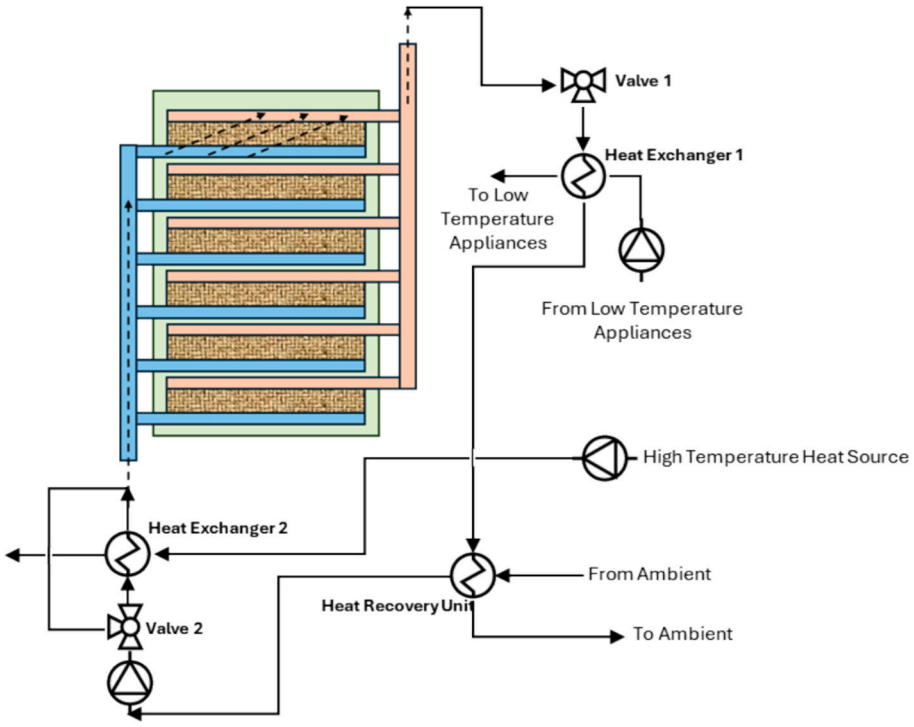

Fig. 9. An open system design based on proposed stacked bed reactor model for space heating application.

integrated into the system, allowing in situ charging of the SIM. In the charge cycle, valve 1 bypasses heat exchange 1 and valve 2 directs the flow via heat exchanger 2 to be heated from a high-temperature source. In the discharge cycle, valve 1 directs the heated flow via heat exchanger 1 after sorption process in order to transport heat to building and later to the heat recovery unit. In discharge cycle, valve 2 bypass the heat exchanger 2.

The experimental results are subsequently used to evaluate the

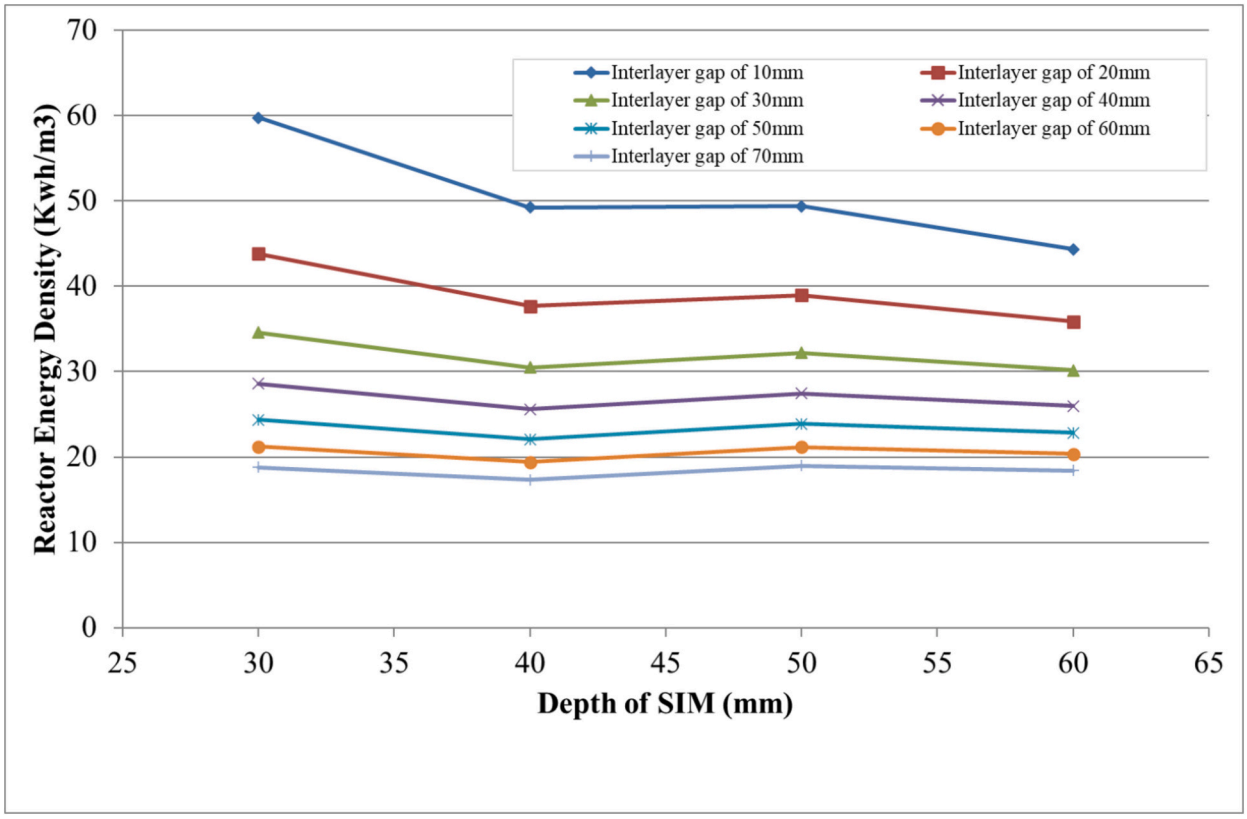

Fig. 10. Variations in reactor energy density for different SIM heights and interlayer gap spacings. The interlayer gap spacing is the combined height of the air gaps at the layer's input and output ($h_{in} + h_{out}$).

preliminary design and varied operational parameters of a stacked bed reactor. Utilisation of heating systems varies dependent upon the end user requirements and consequently the heating strategy applied. For the current case, maximised use of the available materials and space is required, hence generating the most efficient overall system in terms of energy output per volume of SIM. As such, four scenarios are investigated, and are described below.

- Scenario 1a: SIM is used for one discharge per day and then recharged via waste heat 25 times before disposal.
- Scenario 1b: SIM is used for one discharge per day and then recharged via waste heat 50 times before disposal.
- Scenario 2a: SIM is used for one discharge over multiple days and then recharged via waste heat 25 times before disposal.
- Scenario 2b: SIM is used for one discharge over multiple days and then recharged via waste heat 50 times before disposal.

In each case, it is assumed that the SIM cassettes are removed, replaced and recharged using waste heat. From the data sets within Figs. 5, 6 and 9 the perceived best utilisation (i.e. maximum energy density and temperature uplift) for a single daily discharge (10 h) will be from a height of thermochemical storage material (h_{tcs}) at 30 mm for each layer of the stacked bed reactor. In a stacked bed reactor however, there are competing requirements where higher energy densities will require a larger number of thinner layers, but this increase in the number of layers requires an increase in the inter-layer void spaces, bed bases and the separators required for each layer. Hence, using the maximum energy density associated with each layer thickness an overall comparison of reactor energy density is presented in Fig. 10 derived from the results in Fig. 6(d) and Eq. (4).

Initial studies focused on 1 m^3 reactor consisting of 3 mm solid insulating interlayer between each layer (h_b) and a 2 mm porous base within each layer separating the inlet (h_p). These were chosen as the cube dimensions are compatible with an Intermediate Bulk Containers (IBC) tank whose transportation and storage has been standardised.

For scenario 1, a single use of SIM and subsequent recharge, with a material whose inherent energy density is 110 kWh/m^3 (30 mm depth, discharge time of 10 h and target uplift temperature of 5 °C), using multiple thin layers with the thinnest interlayer gap (10 mm consisting of 5 mm above (h_{out}) and 5 mm below (h_{in})) provides real reactor energy densities of between 20 and 60 kWh/m^3. Increasing the thickness of the layer has a detrimental impact on the overall energy density, i.e. multiple thin layers provide the most efficient energy density.

Table 4 shows number of SIM layers in 1m^3 of stacked bed reactor and total volume of SIM within that specfic design. Using acquired the energy density data (Fig. 6) for each SIM height the optimal reactor layout has 18 layers at 30 mm SIM height, with an interlayer gap of 10 mm. The least effective configuration is from a 60 mm SIM height and interlayer gap of 70 mm resulting in an overall reactor with 25 % of the available energy of the best configuration.

For the second scenario where a single discharge is completed over multiple days, Table 3 highlights that a discharge time of 43.07 h is the maximum usage period before the temperature uplift falls below the cut off point of 5 °C. This test considered a timescale which would allow almost full discharge cycle and significantly improved utilisation of the SIM. The evaluated inherent energy density from experiment is 241.7 kWh/m^3 and using 11 thin layers with the thinnest interlayer gap (10 mm consisting of 5 mm above (h_{out}) and 5 mm below (h_{in})) provides an optimum real reactor energy density of 159.5 kWh for 60 mm of SIM (Fig. 11). Conversely, with an interlayer gap of 70 mm, the energy density is reduced to 58.8 kWh/m^3.

3.2.1. Modelling the potential carbon footprint impact of the reactor variations

The case example of a single space cabin (L = 9.87 m, W = 4.25 m and H = 3.04 m) with mineral wool insulated cladding material (U-value of 0.16) is examined in under UK climate classifications with a target internal temperature of 20 °C, ground temperature of 8 °C and UK heating degree day base temperature of 16.3 °C and heating power required at −1 °C. The heating degree days (HDD) are calculated from daily temperature data from 2012. Estimation for the heating load of the building is based upon the CIBSE TM41b approach, as per Eq. (6).

$$\text{Heat load (kWh)} = \text{Heat loss coefficient } \left(\text{kW·K}^{-1}\right) \times \text{degree days (K·day)} \times 24 \left(\text{h·day}^{-1}\right) \quad (6)$$

For this case example, total heat loss from building to air and ground are calculated based on presented values in Table 5 and is 0.11 kW/K. The calculated values for mentioned parameters by considering HDD of 2468 are 0.2 kW and 0.7 kW, respectively.

Fig. 12 shows the heat load required to maintain an internal temperature of 20 °C during daily operations. By evaluating the different reactor configuration options, the optimum utilisation of SIM can be determined.

Utilising data of the best-case scenario of single use (30 mm SIM height, 10 mm interlayer gap), the worst-case scenario of single use (60 mm SIM height, 70 mm interlayer gap) and the multi-discharge case it is also possible to calculate the equivalent mass of SIM required to cover the monthly building heat demand, which is also shown in Fig. 12. Clearly, the multi-use methodology uses significantly less SIM, an annual total of 2430 kg compared to 5356 kg and 9334 kg with the single use scenarios potentially reducing both the overall cost and impact on the environment. Applying the use case conditions, recharging of SIM after either 25 or 50 cycles, reduces the actual volume of fresh material required to 291 kg and 194 kg for scenario 1a, 388 kg and 215 kg for scenario 1b, and 119 kg for scenarios 2a and b over the first year. Over multiple years the SIM used in the 25 charge cycle is double that of the 50 charge cycle.

The impact on the carbon footprint due to the proposed change from

Table 4
Stacked bed reactor design parameters and related specific energy density.

SIM height	Interlayer gap spacing (h_{in} + h_{out})	Number of SIM layer in 1m^3	Volume of SIM in reactor	Maximum specific energy density at 40 lpm – 10 h discharge	Full discharge status after 10 h
[mm]	[mm]		[m^3]	[kWh/m^3]	
30	10	18	0.54	59.2	Yes
	20	13	0.39	42.7	
	30	10	0.30	32.9	
	40	8	0.24	26.3	
	50	7	0.21	23.0	
	60	6	0.18	19.7	
	70	5	0.15	16.4	
40	10	15	0.60	48.0	No
	20	11	0.44	35.2	
	30	9	0.36	28.8	
	40	8	0.32	25.6	
	50	6	0.24	19.2	
	60	6	0.24	19.2	
	70	5	0.20	16.0	
50	10	13	0.65	48.1	No
	20	10	0.50	37	
	30	8	0.40	29.6	
	40	7	0.35	25.9	
	50	6	0.30	22.2	
	60	5	0.25	18.5	
	70	5	0.25	18.5	
60	10	11	0.66	41.5	No
	20	9	0.54	33.9	
	30	8	0.48	30.2	
	40	6	0.36	22.6	
	50	6	0.36	22.6	
	60	5	0.30	18.8	
	70	4	0.24	15.1	

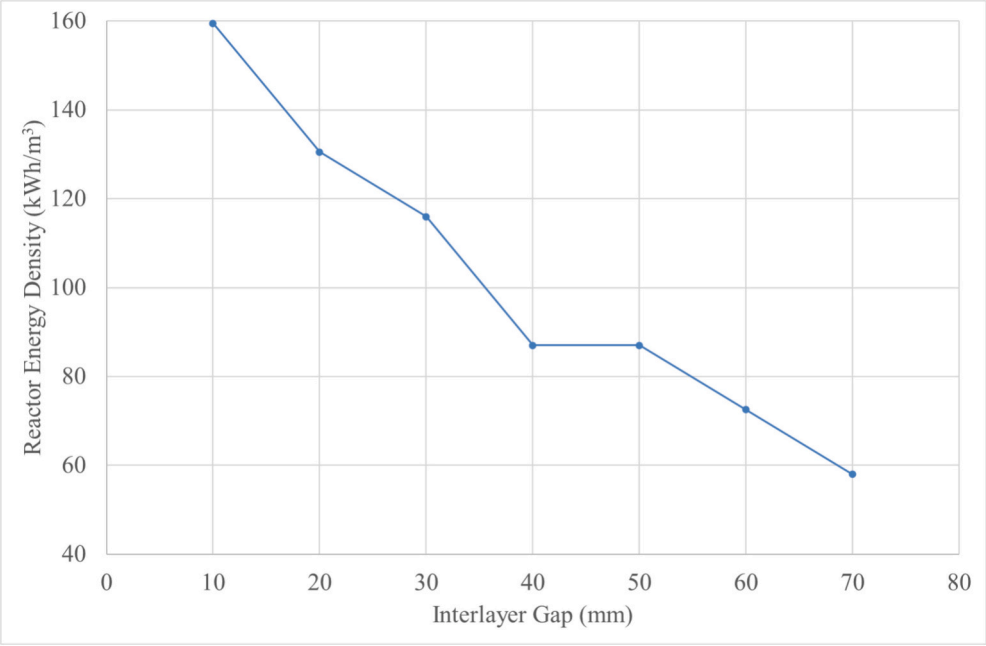

Fig. 11. The impact of interlayer gap spacing (h_{in} + h_{out}) on energy density of the SIM height of 60 mm.

Table 5
Geometries and parameters of simulation model for single space building with volume of 41.9m^3.

Parameter	Building surfaces						Window
	Roof	Wall 1	Wall 2	Wall 3	Wall 4	Floor	
Material	Insulated cladding						
Length [m]	9.87	9.87	9.87	4.25	4.25	9.87	1.3
Width [m]	4.25	3.04	3.04	3.04	3.04	4.25	2.0
Net Area [m^2]	41.9	27.4	30.2	12.9	12.9	41.9	2.6
U Value [W/m$^{2\circ}$C]	0.16	0.16	0.16	0.16	0.16	0.16	3.2
Heat Loss [W/°C]	6.7	4.38	4.80	2.06	2.06	6.70	8.32

fossil fuel heating to renewable heating has been evaluated using the LCA Calculator, allowing a phased approach from the extraction of raw materials, through processing and up to the end use. The reactor walls are constructed from steel and the SIM trays from Polycarbonate. The CO_2 emissions per tonne material for the individual elements of SIM synthesis and reactor build are shown in Table 6, and the final impact figures per kWh and tonne used are shown in Table 7.

Utilising the data from Tables 6 and 7 allows the annual cumulative CO_2 impact for each scenario to be presented alongside the equivalent from both electrically driven and gas driven heating alternatives, and this is presented in Table 8. In each of the scenarios involving the thermal storage the annual total is the sum of 1.) The embodied CO_2 for the reactor materials and construction (accounted for in year 1), 2. The number of SIM replacements required each year (1 replacement every 25 or 50 cycles) and 3.) nominal transport to and from the industrial process for charging (4 mile round trip).

Over a 10 year period the potential environmental benefits of replacing traditional heating systems with Industrial Waste Heat Recovery (IWHR) and thermal storage are clear. The best case (scenario 2b) has an almost 6 times better CO_2 impact over electrical heating and almost 7 times better than gas. Even the worst case (Scenario 1b) is 3 times better than electricity and over 3.5 times better than gas. The largest single impact upon the thermal storage systems is the embodied CO_2 within the reactor configurations. This varies between 569 kg CO_2 and 1059 kg CO_2, with the largest value in the preferential configurations (wrt energy density). This is a result of the increased number of trays required, and polycarbonate having a high embodied CO_2. Beyond year 1, the resulting variations are a function of the number of replacement batches of fresh SIM required and the number of required trips to recharge the material set. As such scenarios 2a and 2b provide the overall best CO_2 impact over the 10 year model. Due to the higher embodied CO_2 in the reactors, it is not until year 7 where Scenario 1a (best) has less CO_2 emitted than Scenario 1a (worst) although the same transition occurs earlier (year 4) in scenario b. When having the best reactor configuration scenario 1b is always preferential to scenario 1a, although in the worst configuration this is reversed. The cumulative CO_2 balance against the electricity and gas scenarios is shown in Fig. 13a and b.

For both the electricity and gas comparisons, the first year of operation for most of the alternative heating systems shows a carbon deficit, only Scenario 1a (worst) in the gas heating scenario being the exception. Beyond that, each alternative scenario is carbon positive against the traditional heating forms although, in the case of scenario 1a and 1b best configurations in the comparison against electricity it is only by 11 and 37 kg respectively. Interestingly, for the second year of operation scenario 1a (worst) returns the overall best CO_2 balance due to the significantly lower embodied carbon within the reactor and it is not until year 7 where scenario 1a becomes the better alternative (wrt CO_2 balance). Both scenario 2a and b are more beneficial from year 3 and continue to be for the remainder of the model duration. Hence, the best configuration of reactor and heating source is very much dependent upon the use case for the portable container. If a temporary structure (<1 year) is envisaged, then fossil fuel heating systems are potentially more environmentally beneficial whereas a more permanent structure with a use period of 3 years and beyond is benefited by heat recovery and thermal storage materials.

4. Conclusions

Experimental and computational investigation has been carried out to study the importance of reactor design of TCS systems on efficient utilisation of thermochemical heat storage materials to improve efficient

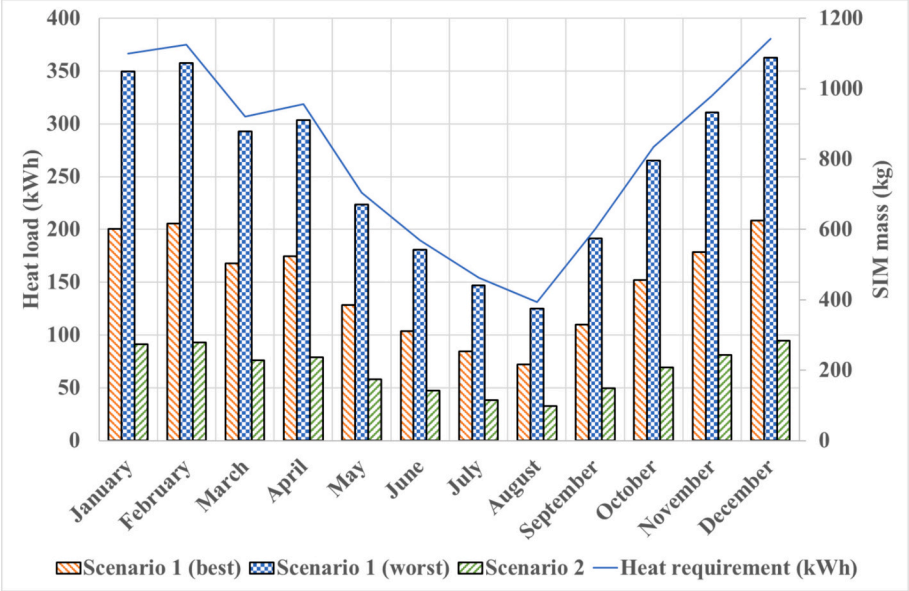

Fig. 12. Total heat loss, heat demand (with/without waste heat stream), estimated waste heat gain and heat stored by TCS for case example.

Table 6
Derived emissions from LCA calculator for system components.

Component	Process	Emissions (kg CO_2/tonne)
Vermiculite	Mining	2.8
	Road transport from mine	16
	Ocean transport	12
	Road transport to end use	7.5
	Mining	1.7
	Processing	89.6
	Road transport from mine	1.3
	Ocean transport	2.7
Calcium chloride	Road transport to end use	4.7
	Frame & walls (steel)	0.4
Reactor multi use	Trays (Polycarbonate)	0.4
	Frame & walls (steel)	0.4
Reactor best single use	Trays (Polycarbonate)	0.7
	Frame & walls (steel)	0.4
Reactor worst single use	Trays (Polycarbonate)	0.2

Table 7
Final carbon impact figures for scenario comparison.

Component	Carbon impact ($kgCO_2$/kWh)	Carbon impact ($kgCO_2$/tonne)
Reactor walls	–	0.44
Trays (Scenario 1 best)		0.12
Trays (Scenario 1 worst)		0.03
Trays (Scenario 2)		0.08
SIM material (Scenario 1 best)	0.22	
SIM material (Scenario 1 worst)	0.38	
SIM material (Scenario 2)	0.1	
Natural gas	0.21	0.16
Electricity	0.18	0.02

energy density and overcome the intermittence of the IWH source. Experimental studies suggest that full discharge cycle (full utilisation of the SIM) needs to be considered as an important factor in reactor design of TCS systems in addition to laboratory parameters such as air flow rate, SIM height and interlayer gap. The results demonstrate that at 40 lpm and 30 mm SIM height, 10 h is sufficient for full utilisation of the available SIM to reach the operational cut off point (minimum uplift of 5 °C) yielding an energy density of 110 kWh/m^3 and a peak temperature uplift of 13 °C. On the contrary, increasing the SIM depth to 60 mm, and maintaining the flow rate reduces the energy density to 60 kWh/m^3, and peak temperature uplift to 13 °C. Therefore, the highest peak temperature is obtained with the thinnest layer of material after 10 h. However, discharge time of 10 h is insufficient to fully discharge the SIM height above 30 mm. Additional experiments revealed that, 43.07 h is required to achieve target uplift temperature of 5 °C for SIM height of 60 mm and calculated inherent energy density from experiment is 241.7 kWh/m^3. The experimental results were subsequently used to evaluate the preliminary design and varied operational parameters of a stacked bed reactor. The aim was to both achieve higher energy density and reduce payback period of proposed stacked bed reactor. The computational study has identified an actual reactor energy density of 159.5 kWh/m^3 which can be achieved with interlayer gap of 10 mm with SIM in 11 layers. LCA analysis has shown that the carbon impact can be significantly varied depending upon reactor configuration, operational use and period of building use. For temporary structures with less than 1 year operation, fossil fuels may be more beneficial, whereas buildings earmarked for long term use will have a significantly improved carbon footprint with the benefit at 10 years being a saving of up to 5000 kg CO_2 against gas hjeating and up to 6000 kg CO_2 when compared with electrical heating.

CRediT authorship contribution statement

S. Hosouli: Writing – review & editing, Writing – original draft, Validation, Methodology, Investigation, Formal analysis, Data curation. **R.J. Sutton:** Investigation, Formal analysis, Data curation, Conceptualization. **J. Searle:** Writing – review & editing, Supervision, Project administration, Funding acquisition. **E. Jewell:** Writing – review & editing, Supervision, Project administration, Funding acquisition, Conceptualization. **J. Elvins:** Writing – review & editing, Supervision, Project administration, Funding acquisition, Conceptualization.

Funding

The authors would like to acknowledge support through the funding of the SPECIFIC Innovation and Knowledge Centre by the Engineering and Physical Science Research Council [EP/N020863/1], Innovate UK [920036], and the European Regional Development Fund [c80892]

Table 8
Annual cumulative CO_2 impact per scenario.

Year	Electricity	Gas	Scenario 1a (best)	Scenario 1a (worst)	Scenario 1b (best)	Scenario 1b (worst)	Scenario 2a	Scenario 2b
1	605	842	1118	698	1105	935	872	872
2	1193	1527	1164	829	1138	1036	895	879
3	1780	2213	1210	953	1171	1138	918	902
4	2368	2898	1256	1083	1204	1245	941	910
5	2955	3583	1314	1214	1237	1347	965	933
6	3543	4269	1360	1338	1270	1448	972	941
7	4130	4954	1406	1468	1303	1556	995	948
8	4718	5640	1452	1599	1336	1657	1018	971
9	5305	6325	1498	1723	1369	1759	1042	979
10	5893	7011	1557	1853	1415	1866	1065	1002

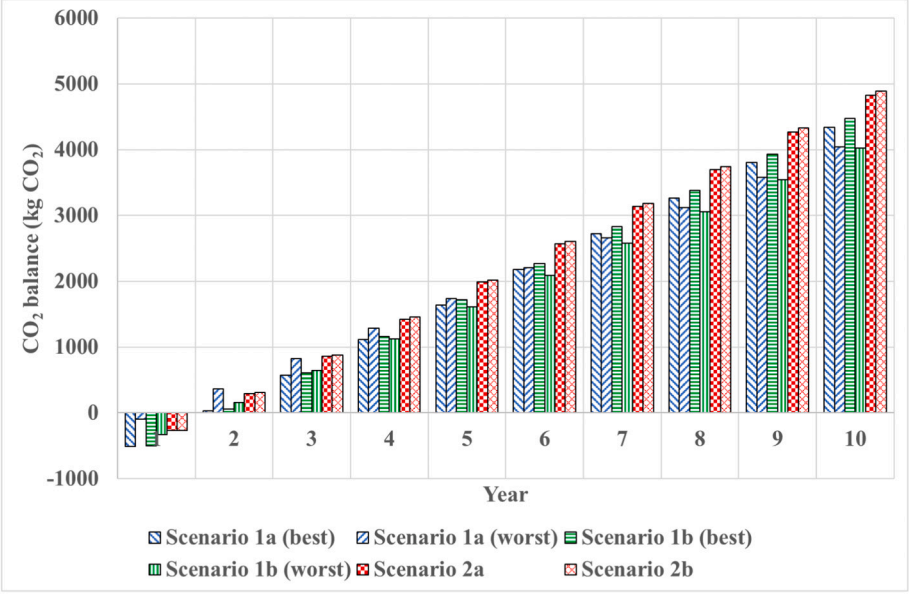

a) Alternative heatingCO_2 balance versus electric heating equivalent

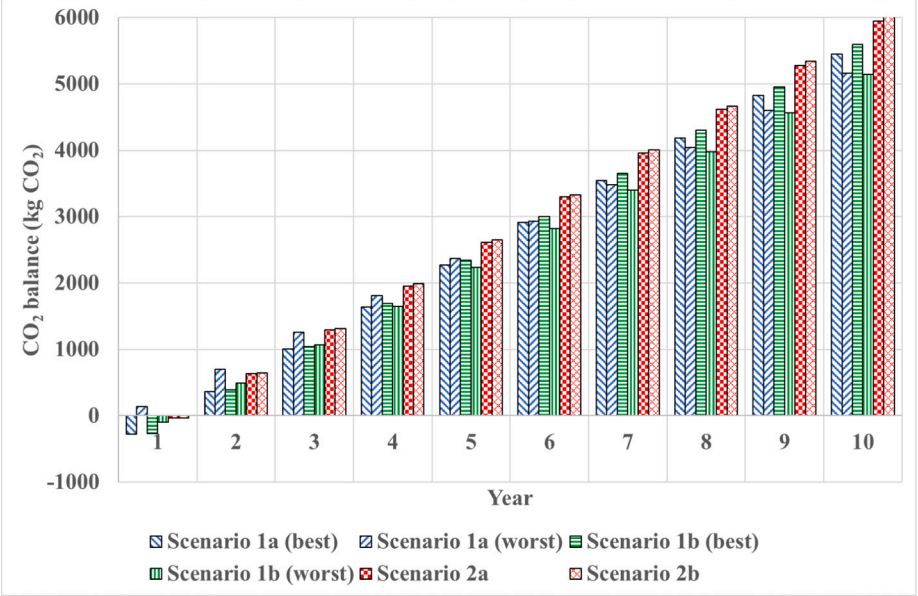

b) Alternative heatingCO_2 balance versus gas heating equivalent

Fig. 13. a Alternative heatingCO_2 balance versus electric heating equivalent.
b Alternative heatingCO_2 balance versus gas heating equivalent.

through the Welsh Government.

Declaration of competing interest

The authors declare that they have no known competing financial interests or personal relationships that could have appeared to influence the work reported in this paper.

Data availability

Data will be made available on request.

References

[1] R. Hanna, R. Gross, B. Parrish, J. Speirs, Best Practice in Heat Decarbonisation Policy: A Review of the International Experience of Policies to Promote the Uptake of Low-Carbon Heat Supply, 2016.
[2] Y. Ding, S.B. Riffat, Thermochemical energy storage technologies for building applications: a state-of-the-art review, Int. J. Low-Carbon Technol. 8 (2013) 106–116.
[3] H. Jouhara, N. Khordehgah, S. Almahmoud, B. Delpech, A. Chauhan, S.A. Tassou, Waste heat recovery technologies and applications, Therm. Sci. Eng. Prog. 6 (2018) 268–289.
[4] P. Stevenson, R. Hyde, Final Report for DECC-The Potential for Recovering and Using Surplus Heat from Industry, 2014.
[5] R. Muhumuza, P. Eames, Decarbonisation of heat: analysis of the potential of low temperature waste heat in UK industries, J. Clean. Prod. 372 (2022) 133759.
[6] IRENA, IRENA–International Renewable Energy Agency [WWW Document], URL, https://www.irena.org/, 2023 (accessed 3.16.23).
[7] B. Mette, H. Kerskes, H. Drück, Concepts of long-term thermochemical energy storage for solar thermal applications–selected examples, Energy Procedia 30 (2012) 321–330.
[8] D. Aydin, S.P. Casey, S. Riffat, The latest advancements on thermochemical heat storage systems, Renew. Sustain. Energy Rev. 41 (2015) 356–367.
[9] H. Kerskes, Thermochemical energy storage, in: Storing Energy, Elsevier, 2016, pp. 345–372.
[10] R.-J. Clark, A. Mehrabadi, M. Farid, State of the art on salt hydrate thermochemical energy storage systems for use in building applications, J. Energy Storage 27 (2020) 101145.
[11] S.K. Henninger, F.P. Schmidt, H.-M. Henning, Water adsorption characteristics of novel materials for heat transformation applications, Appl. Therm. Eng. 30 (2010) 1692–1702.
[12] K. Posern, C. Kaps, Calorimetric studies of thermochemical heat storage materials based on mixtures of MgSO4 and MgCl2, Thermochim. Acta 502 (2010) 73–76.
[13] D. Aydin, S.P. Casey, S. Riffat, The latest advancements on thermochemical heat storage systems, Renew. Sustain. Energy Rev. 41 (2015) 356–367.
[14] P.A.J. Donkers, L.C. Sögütoglu, H.P. Huinink, H.R. Fischer, O.C.G. Adan, A review of salt hydrates for seasonal heat storage in domestic applications, Appl. Energy 199 (2017) 45–68.
[15] L. Scapino, H.A. Zondag, J. van Bael, J. Diriken, C.C.M. Rindt, Sorption heat storage for long-term low-temperature applications: a review on the advancements at material and prototype scale, Appl. Energy 190 (2017) 920–948.
[16] L.G. Gordeeva, Y.I. Aristov, Composites 'salt inside porous matrix' for adsorption heat transformation: a current state-of-the-art and new trends, Int. J. Low-Carbon Technol. 7 (2012) 288–302.
[17] A.R. TUD, Seasonal sorption heat storage–research on thermochemical materials and storage performance, in: Proceedings of Heat Powered Cycles Conference, 2012.
[18] V.M. van Essen, H.A. Zondag, J. Gores, L.P.J. Bleijendaal, M. Bakker, R. Schuitema, W.G.J. van Helden, Z. He, C.C.M. Rindt, Characterization of MgSO4 hydrate for thermochemical seasonal heat storage, J. Sol. Energy Eng. 131 (2009).
[19] C. Ferchaud, Experimental Study of Salt Hydrates for Thermochemical Seasonal Heat Storage, Technische Universiteit Eindhoven, 2016.
[20] K. Linnow, M. Niermann, D. Bonatz, K. Posern, M. Steiger, Experimental studies of the mechanism and kinetics of hydration reactions, Energy Procedia 48 (2014) 394–404.
[21] P.A.J. Donkers, L. Pel, O.C.G. Adan, Experimental studies for the cyclability of salt hydrates for thermochemical heat storage, J. Energy Storage 5 (2016) 25–32.
[22] E.A. Brunberg, The Tepidus System for Seasonal Heat Storage and for Cooling, 1980.
[23] R. de Boer, W.G. Haije, J.B.J. Veldhuis, Determination of structural, thermodynamic and phase properties in the Na2S–H2O system for application in a chemical heat pump, Thermochim. Acta 395 (2002) 3–19.
[24] F. Trausel, A.-J. de Jong, R. Cuypers, A review on the properties of salt hydrates for thermochemical storage, Energy Procedia 48 (2014) 447–452.
[25] Q. Huang, G. Lu, J. Wang, J. Yu, Thermal decomposition mechanisms of MgCl2· 6H2O and MgCl2· H2O, J. Anal. Appl. Pyrolysis 91 (2011) 159–164.
[26] C. Ferchaud, H.A. Zondag, R. de Boer, C.C.M. Rindt, Characterization of the sorption process in thermochemical materials for seasonal solar heat storage application, in: Proceedings of the 12th International Conference on Energy Storage, Lleida, Spain, 2012.
[27] H.U. Rammelberg, T. Schmidt, W. Ruck, Hydration and dehydration of salt hydrates and hydroxides for thermal energy storage-kinetics and energy release, Energy Procedia 30 (2012) 362–369.
[28] H.U. Rammelberg, J.K. Köllner, T. Schmidt, O. Opel, W. Ruck, Hydration and dehydration of salt hydrates and hydroxides for thermal energy storage kinetics, energy release and cyclability, Appl. Energy 154 (2015).
[29] P.A.J. Donkers, L. Pel, O.C.G. Adan, Experimental studies for the cyclability of salt hydrates for thermochemical heat storage, J. Energy Storage 5 (2016) 25–32.
[30] F. Bertsch, B. Mette, S. Asenbeck, H. Kerskes, H. Müller-Steinhagen, Low Temperature Chemical Heat Storage–An Investigation of Hydration Reactions, Proceeding of Effstock, New Jersey, 2009.
[31] B. Michel, N. Mazet, S. Mauran, D. Stitou, J. Xu, Thermochemical process for seasonal storage of solar energy: characterization and modeling of a high density reactive bed, Energy 47 (2012) 553–563.
[32] B. Michel, N. Mazet, P. Neveu, Experimental investigation of an innovative thermochemical process operating with a hydrate salt and moist air for thermal storage of solar energy: global performance, Appl. Energy 129 (2014) 177–186.
[33] F. Trausel, A.-J. de Jong, R. Cuypers, A review on the properties of salt hydrates for thermochemical storage, Energy Procedia 48 (2014) 447–452.
[34] M. Gaeini, A.L. Rouws, J.W.O. Salari, H.A. Zondag, C.C.M. Rindt, Characterization of microencapsulated and impregnated porous host materials based on calcium chloride for thermochemical energy storage, Appl. Energy 212 (2018) 1165–1177, https://doi.org/10.1016/j.apenergy.2017.12.131.
[35] R. Sutton, E. Jewell, J. Searle, J. Elvins, Discharge performance of blended salt in matrix materials for low enthalpy thermochemical storage, Appl. Therm. Eng. 145 (2018) 483–493, https://doi.org/10.1016/j.applthermaleng.2018.09.052.
[36] R.J. Sutton, E. Jewell, J. Elvins, J.R. Searle, P. Jones, Characterising the discharge cycle of CaCl2 and LiNO3 hydrated salts within a vermiculite composite scaffold for thermochemical storage, Energ. Buildings 162 (2018) 109–120.
[37] S. Walsh, J. Reynolds, B. Abbas, R. Woods, J. Searle, E. Jewell, J. Elvins, Assessing the Dynamic Performance of Thermochemical Storage Materials, 2020.
[38] P. Pradyot, Handbook of Inorganic Chemicals, 2002.
[39] H.U. Rammelberg, T. Schmidt, W. Ruck, Hydration and dehydration of salt hydrates and hydroxides for thermal energy storage-kinetics and energy release, Energy Procedia 30 (2012) 362–369.
[40] G. Krese, V. Butala, U. Stritih, Thermochemical seasonal solar energy storage for heating and cooling of buildings, Energ. Buildings 164 (2018) 239–253.
[41] V.M. van Essen, J. Cot Gores, L.P.J. Bleijendaal, H.A. Zondag, R. Schuitema, M. Bakker, W.G.J. van Helden, Characterization of Salt Hydrates for Compact Seasonal Thermochemical Storage, 2009.
[42] P. Tatsidjodoung, N. le Pierrès, L. Luo, A review of potential materials for thermal energy storage in building applications, Renew. Sustain. Energy Rev. 18 (2013) 327–349.
[43] M. Rommel, A. Hauer, W. van Helden, IEA SHC task 42/ECES annex 29 compact thermal energy storage, Energy Procedia 91 (2016) 226–230.
[44] W.G.J. van Helden, M. Bakker, A. Hauer, Compact thermal energy storage: material development for system integration, in: 19. OTTI Symposium Thermische Solarenergie, Bad Staffelstein, Germany, 6–8 Mei 2009, ECN, 2009, pp. 6-p.
[45] G. Zsembinszki, A. Solé, C. Barreneche, C. Prieto, A.I. Fernández, L.F. Cabeza, Review of reactors with potential use in thermochemical energy storage in concentrated solar power plants, Energies (Basel) 11 (2018) 2358.
[46] B. Zettl, G. Englmair, W. Somitsch, An open sorption heat storage concept and materials for building heat supply, Energy Procedia 73 (2015) 297–304.
[47] Y.I. Aristov, Challenging offers of material science for adsorption heat transformation: a review, Appl. Therm. Eng. 50 (2013) 1610–1618.
[48] M.M. Tokarev, Y.I. Aristov, Selective water sorbents for multiple applications, 4. CaCl2 confined in silica gel pores: sorption/desorption kinetics, React. Kinet. Catal. Lett. 62 (1997) 143–150.
[49] S.P. Casey, J. Elvins, S. Riffat, A. Robinson, Salt impregnated desiccant matrices for 'open' thermochemical energy storage—selection, synthesis and characterisation of candidate materials, Energ. Buildings 84 (2014) 412–425.
[50] W. Guan, J. Li, T. Qian, X. Wang, Y. Deng, Preparation of paraffin/expanded vermiculite with enhanced thermal conductivity by implanting network carbon in vermiculite layers, Chem. Eng. J. 277 (2015) 56–63.
[51] M.M. Tokarev, J.V. Veselovskaya, H. Yanagi, Y.I. Aristov, Novel ammonia sorbents "porous matrix modified by active salt" for adsorptive heat transformation: 2. Calcium chloride in ACF felt, Appl. Therm. Eng. 30 (2010) 845–849.
[52] C.Y. Tso, C.Y.H. Chao, Activated carbon, silica-gel and calcium chloride composite adsorbents for energy efficient solar adsorption cooling and dehumidification systems, Int. J. Refrig. 35 (2012) 1626–1638.
[53] R.G. Oliveira, R.Z. Wang, A consolidated calcium chloride-expanded graphite compound for use in sorption refrigeration systems, Carbon N Y 45 (2007) 390–396.
[54] K. Wang, J.Y. Wu, R.Z. Wang, L.W. Wang, Composite adsorbent of CaCl2 and expanded graphite for adsorption ice maker on fishing boats, Int. J. Refrig. 29 (2006) 199–210.
[55] Q. Zhao, J. Lin, H. Huang, Q. Wu, Y. Shen, Y. Xiao, Optimization of thermochemical energy storage systems based on hydrated salts: a review, Energ. Buildings 244 (2021) 111035.
[56] M.M. Farid, A.M. Khudhair, S.A.K. Razack, S. Al-Hallaj, A review on phase change energy storage: materials and applications, Energ. Conver. Manage. 45 (2004) 1597–1615.
[57] Q. Touloumet, L. Silvester, L. Bois, G. Postole, A. Auroux, Water sorption and heat storage in CaCl2 impregnated aluminium fumarate MOFs, Solar Energy Mater. Solar Cells 231 (2021) 111332.

[58] A.J. Carrillo, J. González-Aguilar, M. Romero, J.M. Coronado, Solar energy on demand: a review on high temperature thermochemical heat storage systems and materials, Chem. Rev. 119 (2019) 4777–4816.
[59] P.A.J. Donkers, L. Pel, O.C.G. Adan, Experimental studies for the cyclability of salt hydrates for thermochemical heat storage, J. Energy Storage 5 (2016) 25–32.
[60] B. Fumey, R. Weber, L. Baldini, Sorption based long-term thermal energy storage–process classification and analysis of performance limitations: a review, Renew. Sustain. Energy Rev. 111 (2019) 57–74.
[61] K. Kant, R. Pitchumani, Advances and opportunities in thermochemical heat storage systems for buildings applications, Appl. Energy 321 (2022) 119299.
[62] A. Solé, I. Martorell, L.F. Cabeza, State of the art on gas–solid thermochemical energy storage systems and reactors for building applications, Renew. Sustain. Energy Rev. 47 (2015) 386–398.
[63] L. Miró, J. Gasia, L.F. Cabeza, Thermal energy storage (TES) for industrial waste heat (IWH) recovery: a review, Appl. Energy 179 (2016) 284–301, https://doi.org/10.1016/J.APENERGY.2016.06.147.
[64] S.N. Nyamsi, M. Lototskyy, I. Tolj, Optimal design of combined two-tank latent and metal hydrides-based thermochemical heat storage systems for high-temperature waste heat recovery, Energies (Basel) 13 (2020) 4216.
[65] Y.I. Aristov, Nanocomposite Sorbents for Multiple Applications, CRC Press, 2020.
[66] S.P. Casey, D. Aydin, S. Riffat, J. Elvins, Salt impregnated desiccant matrices for 'open' thermochemical energy storage—Hygrothermal cyclic behaviour and energetic analysis by physical experimentation, Energ. Buildings 92 (2015) 128–139.
[67] N. Janotte, E. Lüpfert, R. Pitz-Paal, K. Pottler, M. Eck, E. Zarza, K.-J. Riffelmann, Influence of measurement equipment on the uncertainty of performance data from test loops for concentrating solar collectors, J. Sol. Energy Eng. 132 (2010).
[68] R.H. Dieck, Measurement Uncertainty: Methods and Applications, ISA, 2007.
[69] J.B. Will, N.P. Kruyt, C.H. Venner, An experimental study of forced convective heat transfer from smooth, solid spheres, Int. J. Heat Mass Transf. 109 (2017) 1059–1067.
[70] S. Walsh, J. Reynolds, B. Abbas, R. Woods, J. Searle, E. Jewell, J. Elvins, Assessing the dynamic performance of thermochemical storage materials, Energies (Basel) 13 (2020) 2202.